

Step and kink dynamics on Au(110) and Pb(111) studied with a high-speed STM

L. Kuipers,* M. S. Hoogeman, and J. W. M. Frenken

*Fundamenteel Onderzoek der Materie—Institute for Atomic and Molecular Physics, Kruislaan 407,
1098 SJ Amsterdam, The Netherlands*

H. van Beijeren

Institute for Theoretical Physics, Utrecht University, P.O. Box 80006, 3508 TA Utrecht, The Netherlands

(Received 14 April 1995)

The dynamics of monoatomic steps on the Au(110) surface is studied with a scanning tunneling microscope from room temperature to 590 K. The time dependence of the position fluctuations of steps was measured as a function of temperature and kink density. The mean-square displacement of the position was found to be proportional to the square root of time, indicating an exchange of atoms with the adjacent terraces. The step dynamics is dominated by the diffusion of geometrically forced kinks that perform a random walk but cannot pass each other. The statistics of step fluctuations in time is mapped on existing theory for one-dimensional diffusion. The resulting atomistic theory explains the time behavior of the mean-square step displacement and its dependence on both temperature and kink density. Kinks that are close together do not move completely independently of each other. The time dependence of the fluctuations of steps on Pb(111) indicates that the step motion of this surface is the result of mass transport along the step.

I. INTRODUCTION

The thermal fluctuation of the position of monoatomic steps on metal and semiconductor surfaces has recently attracted much attention, both experimental^{1–10} and theoretical.^{11–14} The dynamics of steps plays a role in growth^{15,16} and in the equilibration of surface structure and morphology.^{17–22} One of the important issues concerns the mechanism by which a step moves. The atomic processes underlying the step dynamics, in particular the extent to which they involve mass transport along steps or over the adjacent terraces, influence the shape of monoatomic islands during growth.^{23,24} By influencing the island shapes, the dynamics at a step has a large impact on the morphology of the film during growth and can, for example, change three-dimensional into two-dimensional growth.²⁵ Because the fluctuations of a step can be changed by the proximity of neighboring steps,¹² a detailed analysis of the dynamics of steps as a function of the average step density on the surface can be used to measure the interaction between steps.⁷

Figure 1 schematically shows several scenarios by which the position of a step can locally change. We distinguish two different categories. In category A the step moves by exchanging atoms with a reservoir of adatoms on the terraces. The scenarios in category B involve no exchange with the terraces. In this case transport of adatoms and/or vacancies along the step itself is responsible for the movement of the step.

With the advent of microscopic techniques such as transmission electron microscopy (TEM),²⁶ reflection electron microscopy (REM),²⁷ low-energy electron microscopy (LEEM),²⁸ and scanning tunneling microscopy,^{29–31} it has become possible to visualize single mono-

atomic steps on surfaces. With REM and LEEM the lateral resolution is limited to approximately 100 Å, but the monoatomic height differences between adjacent terraces on the surface are clearly resolved. The scanning tunneling microscope (STM) has the spatial resolution to atomically resolve a step.³¹ The STM is therefore ideally suited for the investigation of the atomic mechanisms underlying the step motion. In the present study we employed an STM, which has been optimized for operation at high imaging speed and high specimen temperatures.³²

In general, the individual processes that are combined in one diffusion scenario have different activation energies, so that their rates can differ by many orders of magnitude. For example, recent calculations based on the embedded-atom method predict that the activation energy for a Cu atom to detach from a kink in a $\langle 110 \rangle$ step on Cu(001) to the neighboring adatom site along the step is 0.75 eV while the activation energy for the Cu atom to move further along the $\langle 110 \rangle$ step is only 0.38 eV.³³ For approximately equal attempt frequencies, this activation energy difference results in a ratio between the rates for kink movement and atom displacement along the step of more than seven orders of magnitude at room temperature. Thus, we expect that at temperatures at which the step moves on a time scale that is accessible with the STM, the individual adatoms move so fast that they cannot be observed with the STM.

So far, step dynamics have been studied with REM, STM, and LEEM.^{1–10} Because it is hard to extract the atomic mechanism for the step dynamics directly from the experimental observations, it is essential to perform a statistical analysis of the fluctuations of the step position and relate the result to theoretical predictions. Recently several formalisms have been developed to describe step

dynamics.^{11,13,14} Bartelt *et al.* have shown, using Langevin equations, that when a step moves according to a scenario in category A, the mean-square displacement of the step increases with time t , proportional to $t^{1/2}$.¹¹ When it moves by a scenario in category B, the mean-square displacement is proportional to $t^{1/4}$. In this way it is possible to draw conclusions about the mechanism of the step dynamics by measuring the mean-square displacement of a step as a function of time.

In this paper we present a STM study of step dynamics on Au(110) and Pb(111). Figure 2(a) shows a ball model of the (1×2) missing-row reconstructed Au(110) surface, containing a monoatomic step with a single kink. The step is of the "clockwise," i.e., (111), type. All the step dynamics on Au(110) described in this chapter concern the low-energy (111)-type step. Figure 2(b) depicts a ball model of a Pb(111) surface with a $[1\bar{1}0]$ step and two kinks.

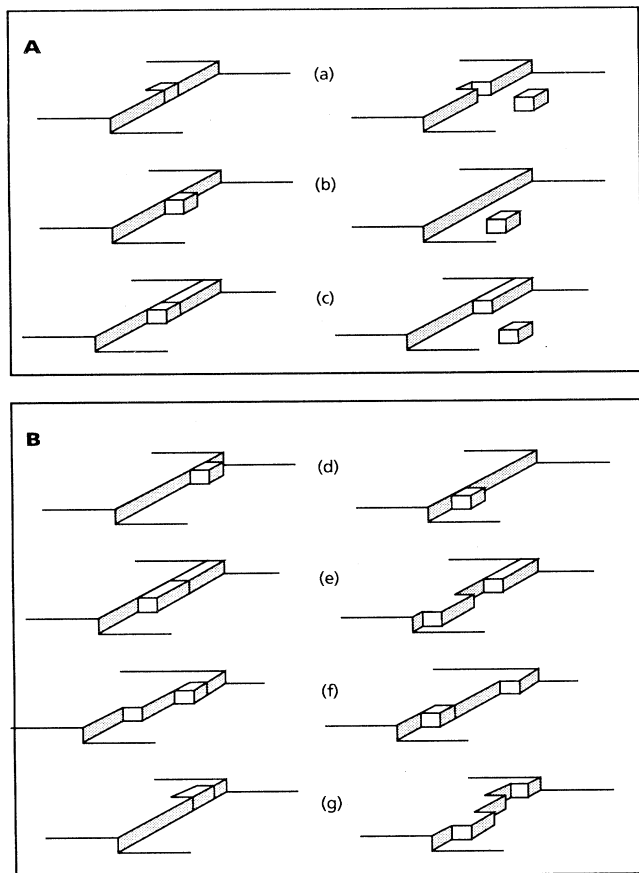


FIG. 1. Schematic illustration of seven scenarios for local displacements of a step on a surface. The scenarios are divided into two categories. Category A contains scenarios in which the step moves by an exchange of one or more atoms between sites on an adjacent terrace and (a) sites in a step, (b) sites at a step, and (c) sites at a kink. Category B contains the scenarios in which the step moves due to a relocation of one or more atoms along the step. (d) Atom diffuses along the step. (e) Exchange of atoms from kink sites and sites at the step, creating a new kink pair. (f) Atom diffuses from one kink to the next. (g) Exchange of one or more atoms in a step sites with sites at the step.

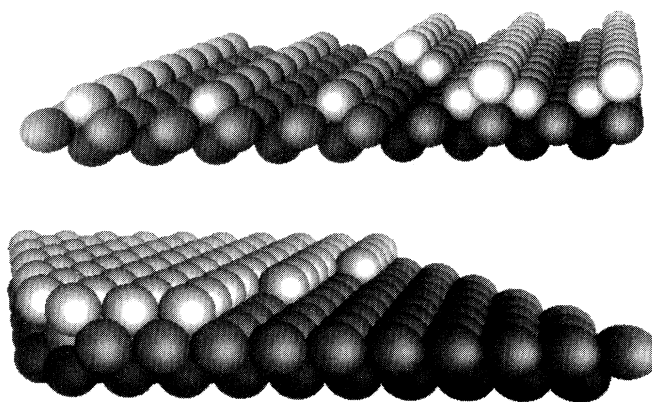


FIG. 2. (a) Schematic model of the (1×2) missing-row reconstructed Au(110) surface. The darker atoms are located in the lower-lying layers. Two terraces are depicted with two complete missing rows on the lower terrace and one on the upper terrace. The clockwise step between the terraces contains one kink. (b) Schematic model of the unreconstructed Pb(111) surface. The darker atoms are located in the lower-lying layers. The image depicts a step along $[1\bar{1}0]$ with two kinks.

From direct observations on Au(110) at relatively low temperatures (from room temperature up to 350 K) we conclude that preexisting kinks in the steps play a crucial role in the dynamics of these steps. By combining this observation with a statistical analysis of the dependence of the mean-square step displacement on time, temperature, and kink density, we develop a model for step dynamics on Au(110) based on the movement of the individual kinks in the steps. This model describes the measurements very well. The mean-square step displacements diverge as $t^{1/2}$, which puts the mechanism for the step fluctuations in category A: exchange of atoms between steps and terraces. By contrast, the mean-square step displacements on Pb(111) show a proportionality to $t^{1/4}$, which indicates that the mass transport involved in the step dynamics on this surface is along the step (category B). We complete our observations with the statistics of the motion of individual kinks on Au(110).

II. EXPERIMENT

A. Cleaning procedure

The Au sample was chemically etched, and mechanically polished. It was cleaned *in situ* by cycles of Ar ion sputtering and annealing to 550 K. The cycles were optimized to produce a sharp (1×2) low-energy electron diffraction pattern with a low background intensity. During the initial stages of sample preparation we found with Auger-electron spectroscopy (AES) that the surface was contaminated with Ca, which segregated from the bulk to the surface. After several tens of cleaning cycles the level of impurities was below the 1% detection limit of AES. By radiative heating of the rear side of the crystal, temperatures up to 590 K were obtained.

The Pb(111) sample was spark-cut from a single-crystal ingot and chemically etched. It was cleaned *in situ* by cycles of AR ion sputtering and annealing to 450 K. After several sputter-anneal cycles the level of contamination of the surface was found to be below the detection limit of AES.

The STM tip was prepared by electrochemical etching of a 0.25-mm-diam W wire and annealing in vacuum. The tip was further prepared *in situ* by field electron emission and Ar ion sputtering.

B. Step shapes: frizziness and pinning

At elevated temperatures the monoatomic steps on Au(110) appear ragged in the STM images. Figure 3 shows such a "rough" step with an average kink density of 0.012 kinks per lattice site, measured at a temperature of 590 K. The vertical stripes in Fig. 3(a) result from the missing-row reconstruction, which is still present at this temperature. The roughness does not reflect the real step shape. Rather it is the result of an under-sampling in time of the step position. In other words, the step position frequently changes within the time needed to scan one line, causing abrupt changes in step position from one scan line to the next. This apparent raggedness has been observed on several metal surfaces, even at room temperature,^{1-3,34-37} and it has been termed "frizziness."¹ At higher line rates (i.e., reduced under-sampling of the step position) the frizziness is reduced. This reduction is illustrated in Fig. 3 where the line rate has been increased from 3.6 Hz [Fig. 3(a)] to 26.1 Hz [3(b)], and 433 Hz [3(c)]. This observation is different from earlier results obtained by Poensgen *et al.*,¹ which seemed to indicate that the frizziness on Ag(111) and Cu(001) was independent of scanning speed.

By decreasing the temperature we reduce the mobility of the steps. In this way we can follow the dynamics of

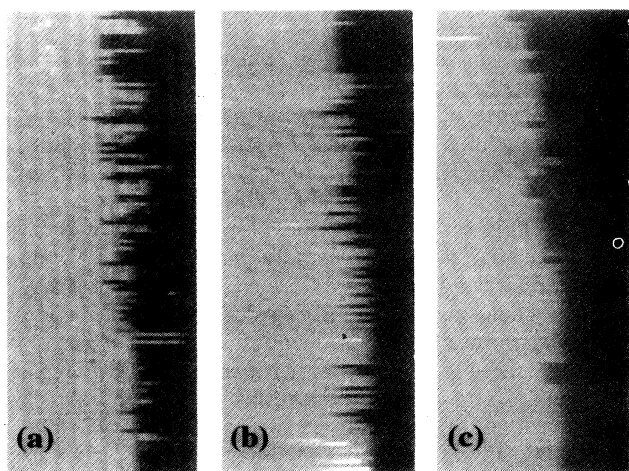


FIG. 3. Three STM images of the Au(110) surface ($102 \text{ \AA} \times 263 \text{ \AA}$, 127 scan lines, $V_t = -0.88 \text{ V}$, $I_t = 0.1 \text{ nA}$) measured at 590 K with different line rates. All three show the same step section. (a) Line rate: 3.6 lines/s. Vertical dark stripes correspond to the missing rows. (b) Line rate: 26.1 lines/s. (c) Line rate: 433 lines/s.

both the steps and the kinks in the steps in "slow motion." Figure 4 shows a sequence of four surface topographs of Au(110), measured at 374 K, at a rate of 1 image every 49 s. The images show three terraces separated by two steps of monoatomic height (one up and one down). The (1×2) missing-row reconstruction of the surface is clearly present on all three terraces. Both steps in Fig. 4 are of the clockwise type. Both steps contain kinks, and the sequence of images in Fig. 4 shows the mobility of the kinks at this temperature. Each movement of a kink causes the position of the step to locally change by one unit of the missing-row reconstruction. When the sampling rate of the step position is slow compared to the mobility of the kinks, this causes the occurrence of apparent kink pairs. Arrows A in Fig. 4(d) indicate such an event, where it appears as if the step contains two nearby kinks of opposite direction. Each time a kink crosses the line being scanned, the image shows a jump in the position of the step. Multiple crossings of the kink through the scan line lead to a typical telegraph noise of the step location (frizziness). We observe that the occurrence of the apparent kink pairs decreases or even disappears completely when the line rate of the measurement is increased sufficiently. At high scan speeds and/or low temperatures (see Fig. 4) we observe that the step dynamics occur only by diffusion of preexisting kinks in the steps. The kinks seem to diffuse freely, but they do not pass each other by more than two atom spacings, thus almost completely avoiding "overhangs" in the step shape. We are forced to conclude that the thermal creation of kink pairs can only play a minor role in the step dynamics (and the frizziness) on Au(110). This is in contrast with the conclusions for Cu(001) and Ag(111) in Refs. 1 and 2.

We find that all the steps on the Au(110) surface are pinned. Arrow B in Fig. 4 indicates the most common pinning center, which appears as a protrusion at a step. We assume that it consists either of one or more Ca

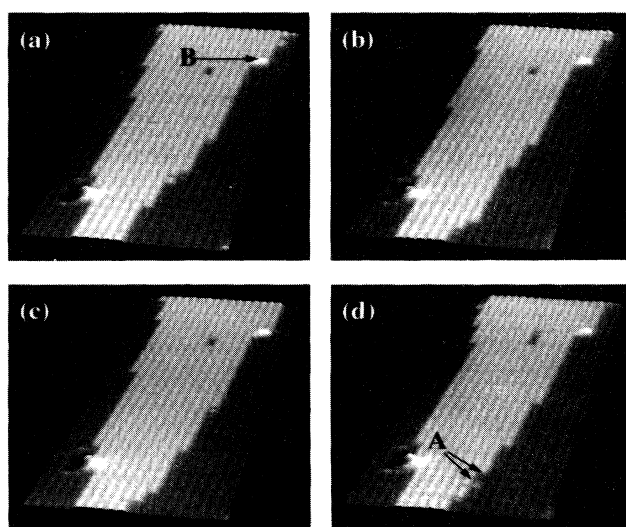


FIG. 4. Sequence of four STM images of the Au(110) surface ($160 \text{ \AA} \times 513 \text{ \AA}$, $V_t = -0.88 \text{ V}$, $I_t = 0.1 \text{ nA}$) measured at 374 K at a rate of 1 image/49 s. Arrows A indicate an apparent kink pair. Arrow B indicates a pinning center.

atoms that have segregated from the bulk to the surface or of one or more Mo atoms that have been sputtered from the sample holder onto the surface. From the STM measurements performed at several temperatures after different cleaning treatments we estimate that the typical density of these protrusions is between 10^{-4} and 10^{-3} monolayer. The average distance between protrusions along a step is 400 Å. Another mechanism by which the step can be pinned on the reconstructed Au(110) surface is the so-called fish-scale pattern that results from a local miscut of the surface towards either $(1\bar{1}0)$ or $(\bar{1}10)$, which effectively pins the step at the junction of two terraces with a height difference of two atomic planes.^{38,39}

If a step on Au(110) is not pinned precisely along the close-packed $[1\bar{1}0]$ surface azimuth, this local misorientation has to be accommodated via geometrically enforced kinks, as is indicated in Fig. 5. The local kink density ρ is the ratio of the number of the enclosed geometrical kinks plus one and the distance between the pinning centers. The step pinning on Au(110) typically leads to step sections with kink densities in the range from 0 to 0.125 kinks/lattice site.

We observe that the number of atoms between the pinning centers is not conserved. This suggests that either the step fluctuations are caused by a direct exchange of atoms between the step and the terraces or that the pinning centers indicated in Fig. 5 pin the step but allow adatoms traveling along the step to diffuse past them. If steps are pinned perfectly along the $[1\bar{1}0]$ direction, the step position between the pinning centers does not move over large time intervals, again demonstrating that

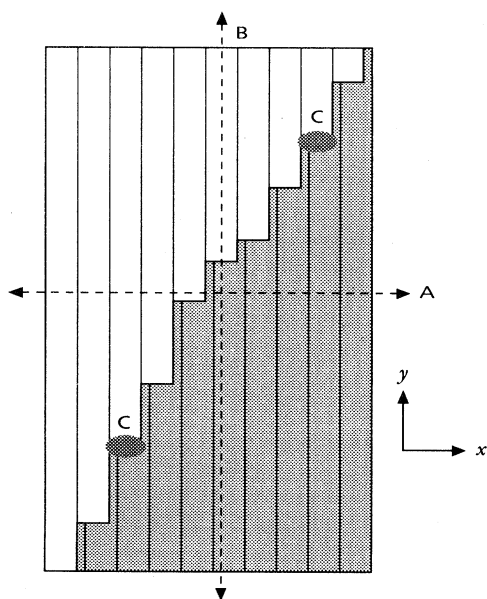


FIG. 5. Schematic illustration of a pinned step on the Au(110) surface. The solid vertical lines indicate the missing-row structure. The step pinned between the pinning centers C contains five geometrical kinks. The dashed arrows indicate the scan lines used in Secs. III and IV for the study of the time fluctuations of, respectively, the steps (arrow A, x direction) and the kinks (arrow B, y direction).

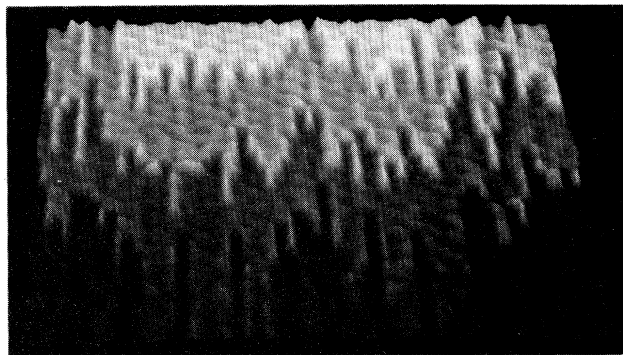


FIG. 6. Atomically resolved STM image of the Pb(111) surface ($63 \text{ \AA} \times 82 \text{ \AA}$, $V_t = +0.15 \text{ V}$, $I_t = 1.0 \text{ nA}$) measured at room temperature in 0.5 s.

thermal kink creation at these temperatures is negligible.

Because the movement of a step is caused by the diffusion of kinks along the step, the pinning centers spectacularly increase the mobility of the step on a short time scale by inducing a superthermal kink density. On a long time scale the mobility of the steps is reduced completely due to the pinning, which sets a maximum amplitude of the step fluctuations.

At room temperature the dynamics of the steps on Pb(111) are so fast that even with the maximum line rate of our STM of 1 kHz the steps remain frizzy. Figure 6 shows a STM image of a section of the Pb(111) surface with four steps. On each of the terraces the atoms are resolved. On Pb(111) it is less easy to determine the location of the pinning centers than on Au(110). In some images they show up as a protrusion similar to the ones observed on Au(110). But usually we can only locate them as the sites in a step that are immobile during a series of STM images.

III. STEP FLUCTUATION STATISTICS

We have shown in Sec. II B that the under-sampling in time of the position of a mobile step leads to the mixing of spatial and temporal information in the STM images. In order to measure exclusively the time dependence of the step fluctuations, we repeatedly scan one individual line perpendicular to the step. Thus we obtain the position of the step as a function of time, for one location along the step, which we usually choose midway between the nearest two pinning centers (scan line A Fig. 5). We suppose that, on a sufficiently short time scale, the central part of a pinned step section fluctuates as if it were part of an infinitely long, free step with the same kink density.

Figure 7 shows the fluctuations in time of two steps measured simultaneously at a temperature of 475 K, displayed as a pseudo-STM image. The vertical axis denotes the lateral coordinate perpendicular to the $[1\bar{1}0]$ direction. The horizontal axis corresponds to time. Figure 7 demonstrates that the position of the steps can be determined with missing-row resolution. In the 32-s time window both steps in Fig. 7 exhibit several abrupt position changes caused by kinks crossing the scan line. The abruptness of the changes in the step position is the result

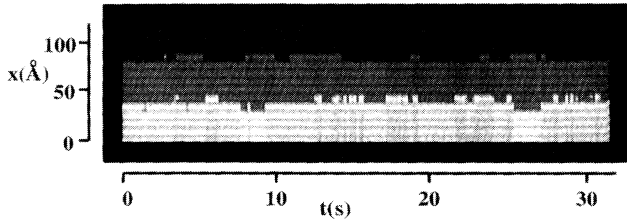


FIG. 7. Time sequence of a scan line across two steps on Au(110), measured at 475 K ($32 \text{ s} \times 118 \text{ \AA}$, $V_t = -0.60 \text{ V}$, $I_t = 0.1 \text{ nA}$). The time per scan line is 83 ms.

of a very low probability of observing the actual moment of the passage of a kink through the scan line. This probability is negligible due to the combination of the discreteness of the kink motion (see Sec. IV), the high resolution of the STM along $[1\bar{1}0]$ (less than the interatomic spacing) and the fact that the time needed for a kink displacement of one lattice unit is probably very short compared to the average time between successive displacements.

In order to quantify the step fluctuations we evaluate the mean-square displacement of the step:

$$\sigma_x^2(t) = \langle [x(t+t_0) - x(t_0)]^2 \rangle, \quad (1)$$

where $x(t)$ is the position of the step at time t and the angular brackets denote an averaging over all time origins t_0 . The x and y directions are perpendicular and parallel to the step. Figure 8 shows a double-logarithmic representation of a typical mean-square displacement as a function of time, for a step with a kink density of 0.0156 kinks/lattice site, measured at 556 K. For the determination of this particular mean-square displacement, the step position was recorded during 0.2 s with a time resolution

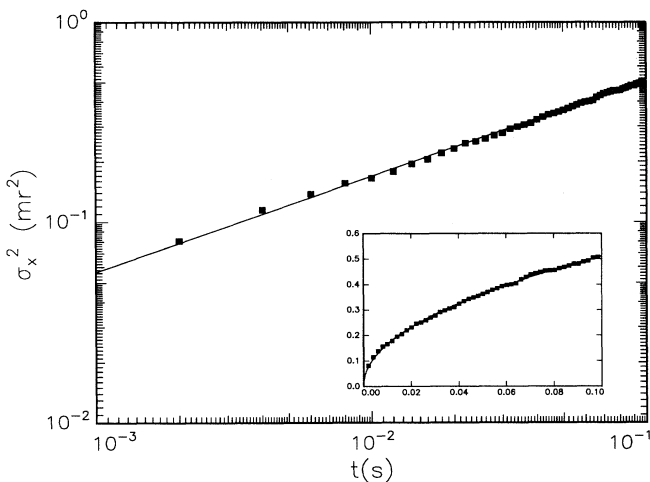


FIG. 8. Double-logarithmic representation of $\sigma_x^2(t)$ of a step on Au(110) with a kink density of 0.0156 kinks/lattice site, at a temperature of 556 K. The mean-square displacement has been expressed in units of the square of the missing-row spacing. The inset shows $\sigma_x^2(t)$ in a linear plot. The solid curves are power-law fits, with $\sigma_x^2(t) \propto t^{1/2}$.

of 2 ms. It is clear that $\sigma_x^2(t)$ follows a power law. We find that the power is 0.48 ± 0.05 for all temperatures and kink densities, where the error margin reflects the standard deviation of the power measured from several tens of step sections. We can therefore write

$$\sigma_x^2(t) = m(\rho, T) t^{0.48 \pm 0.05}, \quad (2)$$

where the prefactor m may depend on the temperature T and the kink density ρ . The power is close to 0.5 over the entire experimentally accessed range of $\sigma_x^2(t)$ (more than one order of magnitude). We therefore conclude that the mean-square displacement of steps on Au(110) is proportional to the square root of time, $t^{1/2}$, which implies that the steps exchange atoms with the terraces (category A) (see Sec. V).

Not only the time dependence but also the dependence of the step fluctuations on the kink density contains information about the mechanism underlying the motion of kinks and steps. From the evaluation of $\sigma_x^2(t)$ for step sections with different kink densities, the dependence of $m(\rho, T)$ on the kink density is determined directly. We find that the step dynamics midway between two pinning centers only depends on the kink density and not on the distance between the pinning centers, from which we conclude that the pinning centers do not strongly affect the step dynamics on the time scale used in this study. Figure 9 shows a double-logarithmic representation of $m(\rho, T)$ vs ρ , for different temperatures. Assuming a power-law dependence, we find that $m(\rho, T)$ is described by

$$m(\rho, T) = c(T) \rho^{0.96 \pm 0.12}, \quad (3)$$

where the proportionality constant c may only depend on temperature. The error bar corresponds to the statistical uncertainty in the slopes in Fig. 9. We conclude that the mean-square displacement of steps on Au(110) is propor-

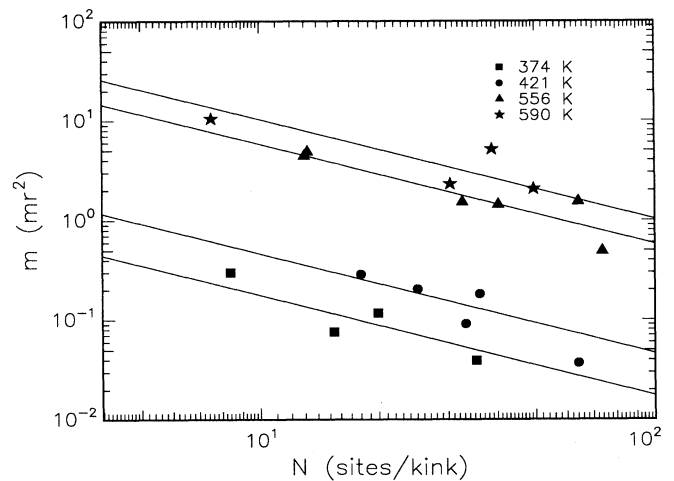


FIG. 9. Double-logarithmic representation of the mean-square displacement prefactor $m(\rho, T)$ vs the average kink distance $N = \rho^{-1}$ for different temperatures on Au(110). The prefactor $m(\rho, T)$ has been expressed in units of the square of the missing-row spacing. The solid lines are fits with $m(\rho, T) \propto c(T)\rho$.

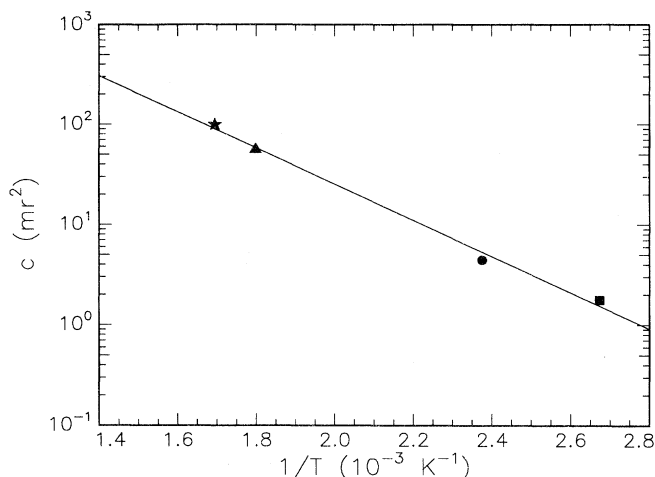


FIG. 10. Arrhenius plot of the prefactor $c(T)$ on Au(110), expressed in units of the square of the missing-row spacing. The solid line is a fit according to $c(T) \propto \exp(-E_{\text{act}}/2k_B T)$, with $E_{\text{act}} = 0.72$ eV.

tional to the kink density.

From Sec. II B we know that the step fluctuations are caused by the motion of kinks. Because the movement of a kink probably is a thermally activated process, we expect $c(t)$ to exhibit Arrhenius behavior. Figure 10 shows an Arrhenius plot of $c(T)$, which confirms our expectation. The slope in Fig. 10 corresponds to an activation energy of 0.7 ± 0.1 eV (see Sec V). This is the activation energy for the movement of a single kink along the step.

The step dynamics on Pb(111) is quantified in the same way as on Au(110). From the step position as a function of time the mean-square step displacement is obtained [Eq. (1)]. Figure 11 is a double-logarithmic representation of the mean-square displacement of a step on Pb(111)

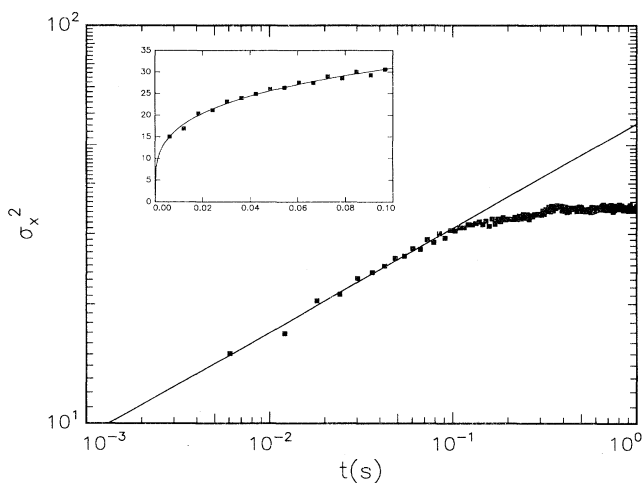


FIG. 11. Double-logarithmic representation of $\sigma_x^2(t)$ of a step on Pb(111) with a kink density of 0.3 kinks/lattice site, at room temperature. The mean-square displacement has been expressed in units of the square of the lattice spacing perpendicular to $[1\bar{1}0]$. The inset shows $\sigma_x^2(t)$ in a linear plot for the first 0.1 s. The solid curves are power-law fits, with $\sigma_x^2(t) \propto t^{1/4}$.

with a kink density of 0.3 kinks/lattice site, measured at room temperature. It shows that the mean-square displacement of steps on Pb(111) for short times also obeys a power law in time. The slope in Fig. 11, however, indicates that the mean-square displacement is proportional to $t^{1/4}$ rather than $t^{1/2}$. We find this for all the steps we investigated on Pb(111) at room temperature. Figure 11 shows that for longer times the mean-square displacement levels off. We suggest that this is caused by step pinning.

IV. KINK DYNAMICS ON Au(110)

A. Single kink fluctuation statistics

Our observation at relatively low temperatures (e.g., Fig. 4) revealed the crucial importance that kinks have in the movement of a step. In this section we investigate the fluctuation of the positions of the kinks directly. Similar to the way in which the step position was measured as a function of time, we measure that of a single kink by repeatedly scanning one individual line along the $[1\bar{1}0]$ direction, which passes through the kink (scan line B in Fig. 5) Figure 12 shows a pseudo-STM image, similar to Fig. 7, of the position of a kink as a function of time measured at 374 K. The horizontal axis corresponds to time and the vertical axis denotes the lateral coordinate along the $[1\bar{1}0]$ direction. The position of the kink is the point where the height abruptly changes by 1.4 Å.

Because the kinks on Au(110) move over one unit of the lattice by the evaporation or the adsorption of two atoms [see Fig. 2(a)], one might expect to observe two types of kinks, the initial or final configuration shown in Fig. 2(a) and an intermediate one where just one atom has left or is attached. The steepness of the height change in Fig. 12 should be different for both types of kinks. We have not succeeded in distinguishing two different slopes at the position of the kink. This either means that the resolution of the tip was not sufficient to observe the difference or that one of the two types is much shorter lived than the other, effectively causing only the long-lives species to be observed.⁴⁰

In order to quantify the diffusive motion of a single kink we use the position of the kink as a function of time to calculate its mean-square displacement:

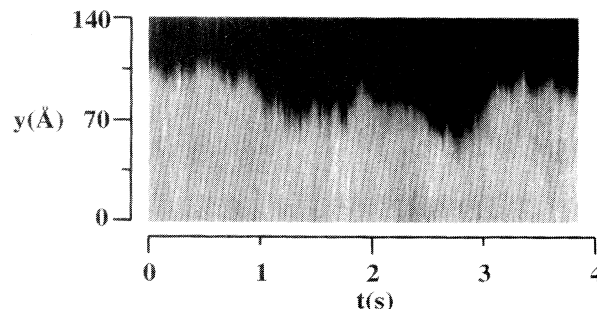


FIG. 12. Time sequence of a scan line across a single kink in a step on Au(110) with an average kink density of 0.021 kinks/lattice site, measured at 374 K (138 Å \times 3.86 s, $V_t = -0.6$ V, $I_t = 0.05$ nA). The time per scan line is 9.7 ms.

$$\sigma_y^2(t) = \langle [y(t+t_0) - y(t_0)]^2 \rangle, \quad (4)$$

where $y(t)$ is the position of the kink as a function of time and the angular brackets again denote averaging over all time origins t_0 . Figure 13 shows a double-logarithmic representation of the mean-square displacement of a kink as a function of time, measured during 2 s with a time step of 0.01 s, at 421 K for a step with a kink density of 0.025 kinks/lattice site. The mean-square displacement follows a power law of time. The exponent found is close to unity, the value expected for an unrestricted random walk. Assuming that the kink in Fig. 13 performs a regular random walk, i.e., $\sigma_y^2(t) = \Gamma(T)t$, and that the jump frequency of the kink $\Gamma(T)$ exhibits Arrhenius behavior with an activation energy equal to 0.7 eV (see Sec. III), we obtain an attempt frequency Γ_0 of 6.3×10^9 Hz. For the temperatures, kink densities, and time scales investigated so far we always find exponents less than unity for the mean-square kink displacement. We interpret this as the hindering effect of neighboring kinks on the diffusive motion of each kink. As will be explained in Sec. V, the mean-square kink displacement should asymptotically become proportional to the square root of time.

B. Correlated and anticorrelated kink motion on Au(110)

The simultaneous measurement of the positions of several kinks as a function of time reveals that the kinks do not always move completely independently from each other. To this end the microscope repeatedly scans a sequence of lines, each running through a different kink. The result of such a measurement is depicted in Fig. 14, which shows the positions of two neighboring kinks as a function of time, measured at 330 K in a step with an average kink density of 0.12 kinks/lattice site. Figure 14

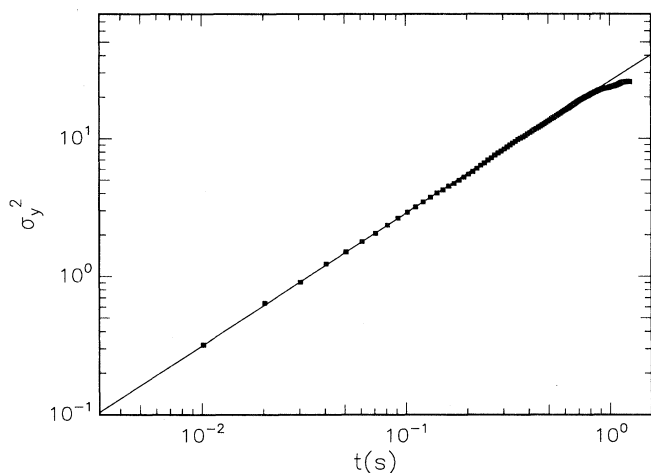


FIG. 13. Double-logarithmic representation of $\sigma_y^2(t)$ of a kink on Au(110) in a step with a kink density of 0.025 kinks/lattice site, at 421 K. The mean-square displacement has been expressed in units of the square of the lattice spacing along $[1\bar{1}0]$. A constant value of 1.0 that resulted from vibrational noise has been subtracted from the mean-square displacement. The solid is power-law fit, with $\sigma_y^2(t) \propto t^{0.95}$.

seems to indicate that when the two kinks happen to be close to each other, their motion is anticorrelated (i.e., the walk that one kink performs is partly the reverse of that of the other kink). This is precisely the behavior that one expects when the kinks move in the following way. Suppose that the position of one of the kinks changes by the evaporation of an atom to a site along the step. This atom diffuses along the step and may reach the next kink, where it then adsorbs. Thus the movement of the two kinks is in opposite directions and, apart from the diffusion time of the evaporated atom, simultaneous [see Fig. 1(f)]. To quantify the degree of correlation in the kink motion, we define a correlation coefficient as

$$\Xi_{12}(\tau) = 2 \frac{\langle \Delta y_1(t_0) \Delta y_2(t_0 + \tau) \rangle - \langle \Delta y_1(t_0) \rangle \langle \Delta y_2(t_0) \rangle}{[(\langle \Delta y_1^2 \rangle - \langle \Delta y_1 \rangle^2)(\langle \Delta y_2^2 \rangle - \langle \Delta y_2 \rangle^2)]^{1/2}}, \quad (5)$$

where $\Delta y_1(t_0)$ and $\Delta y_2(t_0 + \tau)$ are kink displacements of, respectively, kink 1 at time t_0 and kink 2 at time $t_0 + \tau$ and the angular brackets denote an averaging over all time origins t_0 . The factor 2 appears because the average product of $\Delta y_1(t_0)$ and $\Delta y_2(t_0 + \tau)$ counts only half of the correlated displacements of kinks 1 and 2 at a time distance τ .

From the positions of the two kinks in Fig. 14 we obtain a correlation coefficient of $\Xi_{12}(\tau) = -0.46 \pm 0.12$, for the minimal time difference of $\tau = 32$ ms (time between subsequent lines) and for distances of zero or one atomic spacing. For larger distances and/or larger time differences the correlation coefficient is zero, within the statistical error of ± 0.12 . A more detailed analysis of the motion of individual kinks and the anticorrelation between neighboring kinks on Au(110) will be reported in a forthcoming publication.⁴⁰

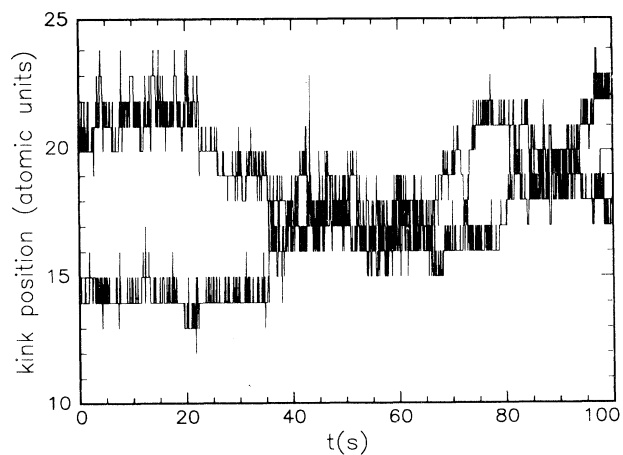


FIG. 14. The positions of two neighboring kinks on Au(110) as a function of time, measured at 330 K. The positions are expressed in units of the lattice spacing along $[1\bar{1}0]$.

V. THEORY FOR Au(110)

In Sec. IV we have found that, on the time scale of our investigation, kinks perform a simple random walk, provided that the neighboring kinks are sufficiently far away. We also know that the kinks cannot pass each other by more than two atom spacings. This leads to a slowing down of their diffusive motion when neighboring kinks are close. Neglecting kink-kink interactions, we model the kinks as particles diffusing on a one-dimensional lattice.

The mean-square displacement of a location along the step, after a time t , is determined by the mean-square difference between the number of kinks that have passed that location in one direction and the number of kinks that have passed in the opposite direction. The passing of the kinks at a certain location along the step cannot be viewed as independent events because of the fact that they cannot pass each other. In order to avoid this complication, we label the kinks. Each time two kinks "meet," we randomize their labels. The labels will therefore perform ordinary, and uncorrelated, random walks even though the kinks themselves obey the noncrossing condition. We now obtain the mean-square displacement of the step from the diffusion of the labels rather than from that of the kinks. The approach is analogous to that taken by van Beijeren, Kehr, and Kutner in the description of tracer diffusion of hard particles on a one-dimensional lattice.⁴¹ The mean-square step displacement after a time t is given by the mean-square difference between the number of labels $n_{lr}(t)$ that have started left from the observation point along the step at $t=0$ and ended up on the right, and the number of labels $n_{rl}(t)$ that have passed in the opposite direction:

$$\sigma_x^2(t) = \langle [n_{lr}(t) - n_{rl}(t)]^2 \rangle. \quad (6)$$

Because the labels perform independent random walks, their mean-square displacement is proportional to t . Therefore $n_{lr}(t)$ and $n_{rl}(t)$ are proportional to $t^{1/2}$, so that the fluctuations on $n_{lr}(t)$, $n_{rl}(t)$, and $n_{lr}(t) - n_{rl}(t)$ are proportional to $t^{1/4}$. This corresponds to a mean-square step displacement proportional to $t^{1/2}$.

In the following we present a more quantitative treatment of the mean-square step displacement. We start from the step velocity autocorrelation function $\langle v_x(t)v_x(0) \rangle$. This is linked to the mean-square step displacement in the following way:

$$\begin{aligned} \frac{d^2}{dt^2} [\sigma_x^2(t)] &= 2 \frac{d}{dt} \langle v_x(t)[x(t) - x(0)] \rangle \\ &= 2 \frac{d}{dt} \langle v_x(0)[x(0) - x(-t)] \rangle \\ &= 2 \langle v_x(0)v_x(-t) \rangle \\ &= 2 \langle v_x(t)v_x(0) \rangle, \end{aligned} \quad (7)$$

where $v_x(t)$ is the velocity of the step at time t . We model the jumps of the step as occurring instantaneously. Therefore it is necessary to define the step velocity at the occurrence of a "jump" in the positive x direction in the following way:

$$v_x(t) = a_x \delta(t - t_{\text{jump}}), \quad (8)$$

where a_x is the lattice constant perpendicular to the step (in the remainder of this paper we will set a_x equal to unity), and t_{jump} is the point in time at which the step jumps. A nonzero velocity at $t=0$ only occurs when the step position jumps precisely at that point in time. Equation (8) describes $x(t)$ correctly. The self-correlation due to the initial jump gives a contribution $2\rho(\Gamma/2)\delta(t)$ to the velocity autocorrelation function, where Γ is the jump frequency of the kinks. The factor 2 is due to the two possible jump directions. The kink density ρ appears as a factor because the step can only jump at $t=0$ if there is a kink next to the observation point on the step, immediately before $t=0$. The frequency Γ with which an isolated kink jumps, to the left or to the right, is assumed to obey the Arrhenius law

$$\Gamma = \Gamma_0 \exp[-E_{\text{act}}/k_B T]. \quad (9)$$

The kink that passes at $t=0$ and makes the step jump at that point in time, will be called the "special" kink in analogy to the special vacancy in Ref. 41. For $t > 0$ a nonzero contribution to the velocity autocorrelation function of the step will only result if at time t the special kink passes the observation point again. In a first approximation, the special kink describes a random walk and therefore the probability of finding it, after a time t , at a distance of n lattice units away from its starting position is given by

$$f(n, t) = e^{-\Gamma t} I_n(\Gamma t), \quad (10)$$

where I_n is a Bessel function of imaginary argument. When the initial move of the special kink was from right to left, the probability for the kink to jump past the observation point at time t equals $1/2\Gamma f(0, t)$ for a move to the right and $1/2\Gamma f(1, t)$ for a move to the left. The contributions to the velocity autocorrelation function due to these moves are $-\rho(\Gamma/2)^2 f(0, t)$ and $\rho(\Gamma/2)^2 f(1, t)$, respectively. When the results of the two possible initial move directions are summed with the self-correlation of the initial move, we arrive at

$$\langle v_x(t)v_x(0) \rangle = 2\rho(\Gamma/2)^2 \{ \delta[(\Gamma/2)t] - f(0, t) + f(1, t) \}. \quad (11)$$

The mean-square step displacement for long times is now directly obtained from the velocity autocorrelation function by integration of Eq. (7):

$$\begin{aligned} \sigma_x^2(t) &= \rho\Gamma \int_0^t d\tau e^{-\Gamma\tau} I_0[\Gamma\tau] \\ &\approx \rho\sqrt{(2/\pi)\Gamma t}. \end{aligned} \quad (12)$$

In the derivation of Eq. (12) we have closely followed a similar derivation in Ref. 41 for the motion of hard particles on a one-dimensional lattice, in the limit of low vacancy density. We have associated the kinks with the vacancies. However, since the kinks move in the y direction, perpendicular to the x direction in which the step moves, we have to "fold" the one-dimensional lattice on which the vacancies and the hard particles diffuse, in or-

der to map it on our kink-step configuration. Figure 15 shows how a step with kinks can be “constructed” from the one-dimensional chain of particles and vacancies. The path length along the step (counting the kinks too) is equal to the chain length.

For arbitrary vacancy densities a more elaborate calculation yields the mean-square particle displacement for both short and long times, with the asymptotic results⁴¹

$$\sigma^2(t) \approx \rho' \Gamma t \quad (\text{small } t) \quad (13a)$$

and

$$\sigma^2(t) \approx \frac{\rho'}{1-\rho'} \sqrt{(2/\pi)\Gamma t} \quad (\text{large } t). \quad (13b)$$

Here, ρ' is the vacancy density. As a result of the chain folding, the kink density ρ is not identical to the vacancy density ρ' , but $\rho = \rho'/(1-\rho')$, so that we finally arrive at

$$\sigma_x^2(t) \approx \frac{\rho}{1+\rho} \Gamma t \quad (\text{small } t) \quad (14a)$$

and

$$\sigma_x^2(t) \approx \rho \sqrt{(2/\pi)\Gamma t} \quad (\text{large } t) \quad (14b)$$

for the mean-square displacement of the step. The crossover between the two time regimes occurs at the time

$$t_x^c \approx (1+\rho)^2 \frac{2}{\pi\Gamma}, \quad (14c)$$

which is approximately equal to the time in which each kink has made, on average, one move. The same approach can be used for the calculation of the mean-square displacement of the kinks themselves. Associating the kinks directly with the hard particles, we obtain for the mean-square kink displacement

$$\sigma_y^2(t) \approx \frac{1}{1+\rho} \Gamma t \quad (\text{small } t) \quad (15a)$$

and

$$\sigma_y^2(t) \approx \frac{1}{\rho} \sqrt{(2/\pi)\Gamma t} \quad (\text{large } t). \quad (15b)$$

The transition time between the two time regimes of the mean-square kink displacement is given by

$$t_y^c = \frac{(1+\rho)^2}{\rho^2} \frac{2}{\pi\Gamma}. \quad (15c)$$

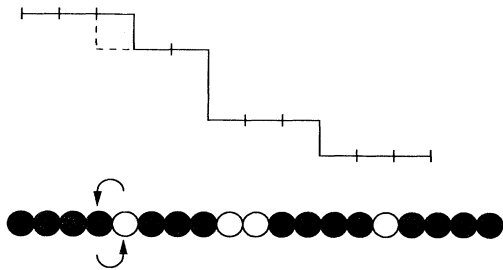


FIG. 15. Schematic illustration of the mapping of a step with kinks onto a linear chain of hard particles with vacancies. Each kink is mapped onto a vacancy (open circle) and each straight step unit is mapped onto a hard particle (solid circle).

This is roughly the time needed for a diffusing kink to cover the distance to one of its neighbors.

It is clear that for the time scales used in this study Eq. (14b) correctly describes both the time dependence of the measured mean-square step displacement (Fig. 8) and its dependence on the kink density ρ and the temperature T (Figs. 9 and 10). Note that due to the square-root dependence of σ_x^2 on the jump frequency of a kink, the slope in Fig. 10 corresponds to half the activation energy for the movement of a kink. The activation energy is that for kink movement by evaporation. Using Eq. (14b) and Fig. 10, we calculate Γ_0 to be $10^{10 \pm 1}$ Hz, which is in good agreement with the value of 6.3×10^9 Hz derived directly from the mean-square kink displacement in Sec. IV A. These numbers are low compared to typical vibration frequencies.

Equation (15a) describes the time fluctuations of kinks on Au(110) well. The fact that all the powers of t , found for the mean-square kink displacement in this study, are less than unity suggests the effect of the crossover to $t^{1/2}$ [Eq. (15b)]. By use of Eqs. (15a) and (15c) the mean-square kink displacement at the crossover time t_y^c is readily calculated. For the kink densities investigated so far (0.01–0.1 kink/lattice site) this crossover value is between 10^2 and 10^4 square lattice spacings. Although these values are far above the maximum mean-square kink displacement in our measurements, a noticeable departure from an exponent of one is expected already at times that are an order of magnitude smaller than t_y^c .⁴¹

When mass transport along the step is responsible for the step dynamics, for example, when the kinks only move by a direct exchange of atoms with neighboring kinks, the long-time dynamics of the steps slows down to a time exponent of $\frac{1}{4}$, according to continuum theory based on the Langevin equation.^{11,14,42} We have not succeeded in deriving a mean-square step displacement proportional to $t^{1/4}$ within the framework of an atomistic model of the type discussed in this section.

In addition to the analytical theory presented here, we have also performed Monte Carlo computer simulations of kink motion along steps. In these simulations we have considered both uncorrelated and anticorrelated motion of neighboring kinks. Furthermore, we have taken into account the effect of the step pinning on the dynamics of the kinks. As expected, the simulations for uncorrelated kink motion lead to $\sigma_x^2(t) \propto t^{1/2}$. However, for anticorrelated motion the simulations show that at the relatively small mean-square displacements used in our study on Au(110) (between 0.05 and 1 square missing-row distance) $\sigma_x^2(t)$ has not yet crossed over fully to $t^{1/4}$, but behaves more like $t^{0.35}$. Nevertheless, from the high experimental value for the exponent of 0.48 ± 0.05 we can still safely conclude that the step fluctuations on Au(110) are the result of uncorrelated kink motion. For σ_x^2 values well above 1, the pinning effect becomes noticeable in the simulations and σ_x^2 levels off, both in the uncorrelated and in the anticorrelated case.

VI. DISCUSSION

We have shown that the movement of steps on Au(110) is the result of the diffusion of preexisting kinks along the

step. The role of nonthermal kinks has also been suggested by a recent study of two vicinal surfaces of Cu(001).³ The surfaces had average step orientations of 7° and 3° with respect to the close-packed [110] azimuth, resulting in steps with kink densities of, respectively, 0.125 and 0.053 kinks/lattice site. This difference in kink density was accompanied by a substantial difference in the frizziness.

The quantitative analysis of the time dependence of the fluctuations in the step positions on Au(110) reveals that the mean-square step displacement is proportional to the square root of time. Our findings can be described with an atomistic model in which the mean-square step displacement is calculated on the basis of uncorrelated diffusion of kinks. The kinks move by evaporation and attachment of atoms. The absence of correlations therefore implies that the kinks exchange atoms with an external reservoir, the terraces, and puts the scenario for the step dynamics in category A. Also the Langevin formalism for step dynamics indicates that the proportionality to $t^{1/2}$ is a fingerprint for a mechanism in category A.¹¹ In this formalism the proportionality constants contains a factor $T/\bar{\gamma}$ in which $\bar{\gamma}$ is the step stiffness. The latter parameter not only contains an entropic contribution, which is important in the present case of forced kinks, but also contains the kink creation probability per site along the step. This means that where our atomistic theory treats steps that fluctuate exclusively due to kink diffusion, the Langevin formalism also incorporates the effect on the step motion of the spontaneous creation and annihilation of kinks.

Recently, the wandering of steps on Si(111) has been measured on a micrometer scale with a resolution perpendicular to the steps of approximately 10 Å. A quantitative analysis of the mean-square step displacements shows that at 1170 K the steps on this surface also move by an exchange mechanism between the steps and the terraces.⁸

For small kink separations we find that the kinks can move in an anticorrelated fashion, indicating a direct exchange of atoms between them. For the Pb(111) surface we find that, for the times accessible in our STM, the mean-square displacement of the steps is proportional to $t^{1/4}$. This time dependence, which was recently also found for steps on Cu(001),⁹ is a fingerprint for a mechanism in which the steps move by mass transport along the steps (category B).¹¹

So far, we have regarded the frequency with which a kink moves as being independent of the (local) kink density. However, on surfaces where the kinks move by mass transport along the step, and the atoms evaporated from a kink perform a random walk along the step, the effective frequency for kink movement should depend on the kink density. This is because the probability for an evaporated atom to reach the neighboring kink before be-

ing recaptured by the kink from which it originated, is equal to one over the number of sites between the kinks (i.e., on average ρ). Thus, we expect that the mean-square step displacement for steps fluctuating with this mechanism will be proportional to $\rho^{5/4}t^{1/4}$.⁴³ In the case that the mean-square step displacement is proportional to $t^{1/4}$, the mean-square kink displacement must also be proportional to $t^{1/4}$ for sufficiently long times. This is because the mean-square displacements of the kinks and the step are geometrically related via the square of the kink density [compare Eqs. (14b) and (15b)].

We think that the mechanism for kink dynamics on Au(110) and Si(111) is the exception rather than the rule. One would expect that "evaporation" of kink atoms to a neighboring step site, followed by one-dimensional diffusion of the atoms along the (close-packed) step between the neighboring kinks, would be the dominant mechanism for kink motion (lowest activation energies). On Au(110) the exchange of kink atoms with the terraces is probably a direct consequence of the missing-row reconstruction, which effectively shields off each kink from the adatoms diffusing in the neighboring missing-row trough.

VII. CONCLUSIONS

Low-temperature observations of the step dynamics on Au(110) show that the step position is changed by the movement of preexisting kinks along the step. The statistics of the step dynamics on Au(110) are mapped on a one-dimensional diffusion model. Both the proportionality of the mean-square step displacement to the square root of time and its proportionality to the kink density indicate that the kinks move by an exchange of atoms with the neighboring terraces. From the temperature dependence of the step fluctuations we find an activation energy for the movement of a kink of 0.7 ± 0.1 eV, which is in reasonable agreement with preliminary calculations based on the effective medium theory.⁴⁴

By studying the movement of the individual kinks on Au(110) we find that they perform random walks along the step. When kinks approach each other to small distances (≤ 1 atom spacing) they frequently exchange atoms with each other. The mean-square displacement of the steps studied at room temperature on Pb(111) scales as $t^{1/4}$. This indicates that the steps on this surface exclusively move due to mass transport along the steps.

ACKNOWLEDGMENTS

We thank G. Mazzeo and B. Mulder for enlightening discussions, and J. F. van der Veen for critically reading the manuscript. This work is part of the research program of the Foundation for Fundamental Research on Matter (FOM) and was made possible by financial support from the Netherlands Organisation for the Advancement of Research (NWO).

*Present address: Dept. of Physics, University of Cambridge, Cavendish Laboratory, Madingley Road, Cambridge CB3 0HE, United Kingdom.

¹M. Poensgen, J. F. Wolf, J. Frohn, M. Giesen, and H. Ibach, *Surf. Sci.* **274**, 430 (1992).

²M. Giesen, J. Frohn, M. Poensgen, J. F. Wolf, and H. Ibach, *J. Vac. Sci. Technol. A* **10**, 2597 (1992).

³J. C. Girard, S. Gauthier, S. Rousset, W. Sacks, S. de Cheveigné, and J. Klein, *Surf. Sci.* **301**, 245 (1994).

⁴N. Kitamura, B. S. Swartzentruber, M. G. Lagally, and M. B.

- Webb, Phys. Rev. B **48**, 5704 (1993).
- ⁵H. Tokumoto, K. Miki, Y. Morita, T. Sato, M. Iwatsuki, M. Suzuki, and T. Fukuda, Ultramicroscopy **42-44**, 816 (1992).
- ⁶S.-I. Kitamura, T. Sato, and M. Iwatsuki, Nature **351**, 215 (1991).
- ⁷C. Alfonso, J. M. Bermond, J. C. Heyraud, and J. J. Métois, Surf. Sci. **262**, 371 (1992).
- ⁸N. C. Bartelt, J. L. Goldberg, T. L. Einstein, E. D. Williams, J. C. Heyraud, and J. J. Métois, Phys. Rev. B **48**, 15453 (1993).
- ⁹M. Giesen-Seibert, R. Jentjens, M. Poensgen, and H. Ibach, Phys. Rev. Lett. **71**, 3521 (1993); M. Giesen-Seibert and H. Ibach, Surf. Sci. **316**, 205 (1994).
- ¹⁰N. C. Bartelt, R. M. Tromp, and E. D. Williams, Phys. Rev. Lett. **73**, 1656 (1994).
- ¹¹N. C. Bartelt, J. L. Goldberg, T. L. Einstein, and E. D. Williams, Surf. Sci. **273**, 252 (1992).
- ¹²N. C. Bartelt, T. L. Einstein, and E. D. Williams, Surf. Sci. Lett. **240**, L591 (1990).
- ¹³G. S. Bales and A. Zangwill, Phys. Rev. B **41**, 5500 (1990).
- ¹⁴A. Pimpinelli, J. Villain, D. E. Wolf, J. J. Métois, J. C. Heyraud, I. Elkinani, and G. Uimin, Surf. Sci. **295**, 143 (1993).
- ¹⁵W. K. Burton, N. Cabrera, and F. C. Frank, Philos. Trans. R. Soc. London Ser. A **243**, 299 (1951).
- ¹⁶J. Villain, J. Phys. (France) **1**, 19 (1991).
- ¹⁷W. W. Mullins, in *Metal Surfaces*, edited by W. D. Robertson and N. A. Gjostein (American Society for Metals, Metals Park, 1963), p. 17.
- ¹⁸J. M. Blakely, *Introduction to the Properties of Crystal Surfaces* (Pergamon, Oxford, 1973).
- ¹⁹H. P. Bonzel, E. Preuss, and B. Steffan, Appl. Phys. A **35**, 1 (1984).
- ²⁰A. Rettori and J. Villain, J. Phys. (Paris) **49**, 257 (1988).
- ²¹M. Ozdemir and A. Zangwill, Phys. Rev. B **42**, 5013 (1990).
- ²²L. Kuipers, M. S. Hoogeman, and J. W. M. Frenken, Surf. Sci. (to be published).
- ²³R. Q. Hwang, J. Schröder, C. Günther, and R. J. Behm, Phys. Rev. Lett. **67**, 3279 (1991).
- ²⁴J. Vrijmoeth, H. A. van der Vegt, J. A. Meyer, E. Vlieg, and R. J. Behm, Phys. Rev. Lett. **72**, 3843 (1994).
- ²⁵H. A. van der Vegt, H. M. van Pinxteren, M. Lohmeier, E. Vlieg, and J. M. C. Thornton, Phys. Rev. Lett. **68**, 3335 (1992).
- ²⁶R. T. Tung and F. Schrey, Phys. Rev. Lett. **63**, 1277 (1989).
- ²⁷N. Osakabe, Y. Tanishiro, and K. Yagi, Surf. Sci. **109**, 353 (1981).
- ²⁸E. Bauer, Ultramicroscopy **17**, 51 (1985).
- ²⁹R. T. Tung and F. Schrey, Phys. Rev. Lett. **63**, 1277 (1989).
- ³⁰X. S. Wang, J. L. Goldberg, N. C. Bartelt, T. L. Einstein, and E. D. Williams, Phys. Rev. Lett. **65**, 2430 (1990).
- ³¹R. S. Becker, J. A. Golovchenko, E. G. McRae, and B. S. Swartzentruber, Phys. Rev. Lett. **55**, 2028 (1985).
- ³²L. Kuipers, R. W. M. Loos, H. Neerings, J. ter Horst, G. J. Ruwiel, A. P. de Jongh, and J. W. M. Frenken, Rev. Sci. Instrum. (to be published).
- ³³M. Breeman and D. O. Boerma, Phys. Rev. B **46**, 1703 (1992).
- ³⁴Y. Kuk, F. M. Chua, P. J. Silverman, and A. J. Meyer, Phys. Rev. B **41**, 12393 (1990).
- ³⁵J. Winterlin, R. Schuster, D. J. Coulman, G. Ertl, and R. J. Behm, J. Vac. Sci. Technol. B **10**, 902 (1991).
- ³⁶S. Rousset, S. Chiang, D. E. Fowler, and D. D. Chambliss, Phys. Rev. Lett. **69**, 3200 (1992).
- ³⁷L. Kuipers and J. W. M. Frenken, Phys. Rev. Lett. **70**, 3907 (1993).
- ³⁸J. K. Gimzewski, R. Berndt, and R. R. Schittler, Surf. Sci. **247**, 327 (1991); Phys. Rev. B **45**, 6844 (1992).
- ³⁹L. Kuipers, Ph.D. thesis, University of Amsterdam, 1994.
- ⁴⁰A preliminary analysis of additional STM measurements of kink motion on Au(110) indicates that the STM images do not distinguish the two different kink shapes. Nevertheless, the motion statistics allow us to separate the two different types of single-atom evaporation/attachment events and determine their activation energies; M. S. Hoogeman, M. F. Chang, L. Kuipers, and J. W. M. Frenken (unpublished).
- ⁴¹H. van Beijeren, K. W. Kehr, and R. Kutner, Phys. Rev. B **28**, 5711 (1983), and references therein.
- ⁴²Due to conservation of the total number of atoms, the motion of kinks will always be anticorrelated on sufficiently long time and length scales, even on Au(110). We therefore expect that on a very long time scale (and in the absence of step pinning) the mean-square displacement of steps and kinks on Au(110) should exhibit a time exponent of $\frac{1}{4}$.
- ⁴³This proportionality is slightly different from our earlier prediction; L. Kuipers, M. S. Hoogeman, and J. W. M. Frenken, Phys. Rev. Lett. **71**, 3517 (1993).
- ⁴⁴M. S. Hoogeman, D. C. Schlöber, L. Kuipers, and J. W. M. Frenken (unpublished).

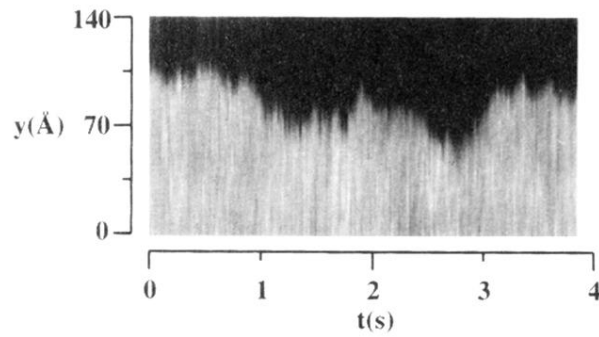


FIG. 12. Time sequence of a scan line across a single kink in a step on Au(110) with an average kink density of 0.021 kinks/lattice site, measured at 374 K ($138 \text{ \AA} \times 3.86 \text{ s}$, $V_t = -0.6 \text{ V}$, $I_t = 0.05 \text{ nA}$). The time per scan line is 9.7 ms.

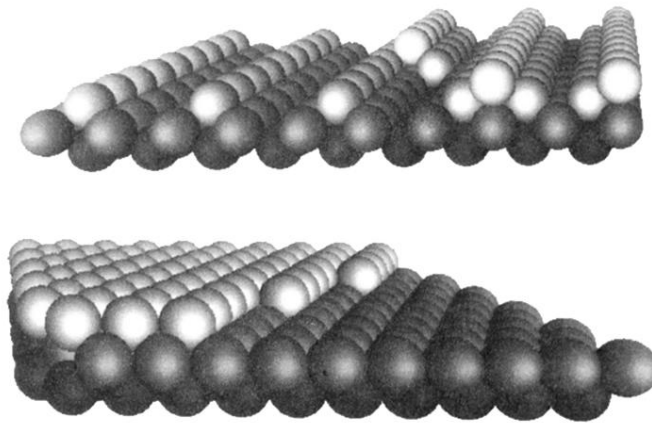


FIG. 2. (a) Schematic model of the (1×2) missing-row reconstructed Au(110) surface. The darker atoms are located in the lower-lying layers. Two terraces are depicted with two complete missing rows on the lower terrace and one on the upper terrace. The clockwise step between the terraces contains one kink. (b) Schematic model of the unreconstructed Pb(111) surface. The darker atoms are located in the lower-lying layers. The image depicts a step along $[1\bar{1}0]$ with two kinks.

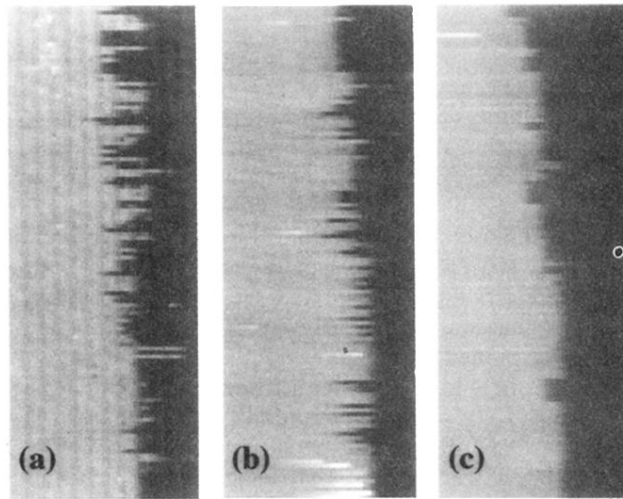


FIG. 3. Three STM images of the Au(110) surface ($102 \text{ \AA} \times 263 \text{ \AA}$, 127 scan lines, $V_t = -0.88 \text{ V}$, $I_t = 0.1 \text{ nA}$) measured at 590 K with different line rates. All three show the same step section. (a) Line rate: 3.6 lines/s. Vertical dark stripes correspond to the missing rows. (b) Line rate: 26.1 lines/s. (c) Line rate: 433 lines/s.

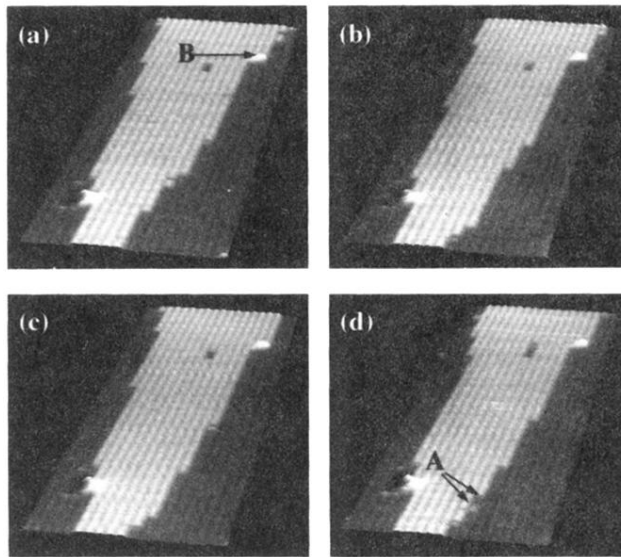


FIG. 4. Sequence of four STM images of the Au(110) surface ($160 \text{ \AA} \times 513 \text{ \AA}$, $V_t = -0.88 \text{ V}$, $I_t = 0.1 \text{ nA}$) measured at 374 K at a rate of 1 image/49 s. Arrows A indicate an apparent kink pair. Arrow B indicates a pinning center.

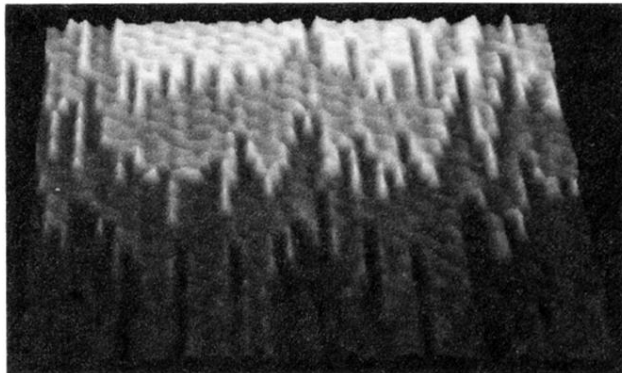


FIG. 6. Atomically resolved STM image of the Pb(111) surface ($63 \text{ \AA} \times 82 \text{ \AA}$, $V_t = +0.15 \text{ V}$, $I_t = 1.0 \text{ nA}$) measured at room temperature in 0.5 s.

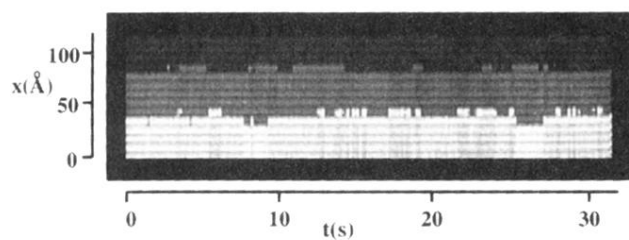


FIG. 7. Time sequence of a scan line across two steps on Au(110), measured at 475 K ($32 \text{ s} \times 118 \text{ \AA}$, $V_t = -0.60 \text{ V}$, $I_t = 0.1 \text{ nA}$). The time per scan line is 83 ms.